Cortical depth-dependent human fMRI of resting-state networks using EPIK

Authors

Patricia Pais-Roldán[1], Seong Dae Yun[1], Nicola Palomero-Gallagher[2-4], N. Jon Shah[1,5-7 *]

[1]Institute of Neuroscience and Medicine 4, Medical Imaging Physics, Forschungszentrum Jülich, Germany

[2]Institute of Neuroscience and Medicine 1, Structural and Functional Organisation of the Brain, Forschungszentrum Jülich, Germany

[3]C. & O. Vogt Institute for Brain Research, Heinrich-Heine-University, 40225 Düsseldorf, Germany

[4]Department of Psychiatry, Psychotherapy and Psychosomatics, Medical Faculty, RWTH Aachen, Aachen, Germany

[5]Institute of Neuroscience and Medicine 11, Molecular Neuroscience and Neuroimaging, JARA, Forschungszentrum Jülich, Germany

[6]JARA - BRAIN - Translational Medicine, Aachen, Germany

[7]Department of Neurology, RWTH Aachen University, Aachen, Germany

Short title: Whole-brain laminar fMRI in humans using EPIK

*** Corresponding author:**

Prof. N. Jon Shah

Institute of Neuroscience and Medicine 4, Medical Imaging Physics, Forschungszentrum Jülich, 52425 Jülich, Germany

Tel: +49 2461 61 6836, Fax: +49 2461 61 8294, Email: n.j.shah@fz-juelich.de

Author Contributions

N.J.S. designed the research; S.Y. developed the MR imaging sequence and the corresponding image reconstruction software; S.Y. and P.P. performed in vivo experiments. P.P. designed and performed all data analysis; P.P. wrote the manuscript and prepared all figures; N.J.S. invented the original EPIK sequence; N.P.-G. verified the anatomical labels and wrote the cytoarchitecture-related discussions; S.Y., N.P.-G. and N.J.S. reviewed the manuscript.

ABSTRACT

Recent laminar-fMRI studies have provided substantial understanding of the *evoked* cortical responses in multiple sub-systems; in contrast, the laminar component of *resting-state networks* spread over the whole brain has been less studied due to technical limitations. Animal studies strongly suggest that the supragranular layers of the cortex play a critical role in maintaining network resonance; however, whether this is true in the human cerebral cortex remains unclear. Here, we used EPIK, which offers unprecedented coverage at sub-millimetre resolution, to investigate cortical broad resting-state dynamics with depth specificity in healthy volunteers. Our results show that human network connectivity is primarily supported by intermediate and superficial layers of the cortex, and that the preferred cortical depth used for communication can vary from one network to another. We validated our results by comparing two resting-state fMRI scans, which were highly consistent, and one task fMRI scan, which exhibited certain laminar differences. The evaluation of laminar-fMRI across the brain encompasses unprecedented computational challenges; nonetheless, it enables a new dimension of the human neocortex to be investigated which may be key in the characterization of neurological disorders from a novel perspective.

Keywords

Cerebral cortex, Cortical Layer, Resting-state fMRI, High-resolution, EPIK

Significance statement

Resting-state networks sustain conscious awareness and diverse cognitive processing in the absence of tasks. In contrast to cortical *areas*, the cortical *depth*-specific signals across different networks have been poorly investigated, mainly due to the small brain coverage enforced in high-resolution imaging methods. Here, using an optimized fMRI sequence, we demonstrate the critical involvement of the supragranular layers of the cerebral cortex in the maintenance of the resting-state dynamics. Given the cytoarchitectonics of the human neocortex, and based on our results, the cortical thickness constitutes an important dimension to characterize the resting-state oscillations in the healthy brain and its functional study may facilitate the identification of novel targets in neurological diseases.

1. INTRODUCTION

In the mammalian brain, the cerebral cortex is organized into specialized functional areas across its surface. In humans, the largest part of the cerebral cortex is occupied by neocortex, where the perikarya of multiple neuronal cell types are organized into six horizontal layers. The layered structure of the neocortex, which can be characterized by its cytoarchitecture, is involved in specialized signal processing [1-3]. The functional specificity of the cortex at its different depths has been demonstrated in animals using multi-site electrodes and, more recently, with cell-specific calcium imaging, e.g., via two-photon microscopy or optical fibers [4-8]. Although electrophysiology can theoretically be performed in the human brain to investigate layer-specific activations, it is an extremely invasive technique and, consequently, data are only available from select patient groups, e.g., in epileptic patients, who benefit from such an undertaking [9]. Moreover, although electrode recordings can provide direct information concerning layer activity, the coverage of electrophysiological recordings is limited by the number of multi-site electrodes which is usually a single point at different depths. In contrast to the limitations of electrophysiology, functional magnetic resonance imaging (fMRI) can afford broad brain coverage non-invasively, although it is usually limited by relatively low spatial resolution. In rodents, experiments merging fMRI and axonal tracing maps demonstrated that layers 2/3, but not other cortical depths, project exclusively to areas within the default mode network [10] and it has been shown that stimulation of upper, but not lower sections of the motor cortex results in network-wide effects [11], suggesting a primary role of the superficial cortical laminae in resting-state networking. Due to a lack of non-invasive methods to sufficiently sample the cerebral cortex, the specific way in which the cortical neurons communicate with each other in the human brain -across different depths and through different areas- largely remains an open challenge, which may be addressed with novel high resolution fMRI methods.

fMRI most commonly relies on the identification of blood changes, which, assuming perfect neuro-vascular coupling, represent neuronal function in the brain [12-14]. Despite its dependence on the vascular architecture of the cortex, laminar fMRI, i.e., sub-millimeter resolution fMRI acquired with the purpose of studying depth-specific neuronal responses, has proven to be a valuable tool for studying cortical dynamics in animals and humans [15-25]. Two main fMRI contrasts are usually employed in human laminar fMRI: cerebral blood volume (CBV), typically applied as part of vascular occupancy schemes (VASO), and blood oxygenation level dependent (BOLD). Although VASO offers high spatial specificity by detecting dilation of the microvasculature based on T1 contrast, it exhibits low sensitivity due to unwanted tissue suppression by an inversion recovery pulse [26-28]. In contrast, sequences based on BOLD present the advantage of a higher signal-to-noise ratio (SNR), with spin-echo-based (SE) echo planar imaging sequences (EPI) offering greater parenchymal specificity and gradient-echo (GE) schemes offering the best sensitivity [27]. The higher SNR and the flexibility to be able to accommodate higher sampling rates makes GE sequences some of the most commonly used in the fMRI field, typically in the form of GE-EPI. Due to GE schemes having enhanced sensitivity to large vessels [29], e.g., pial veins, with long T2* constants, several methods have been presented for use in the pre-processing pipeline to ameliorate contamination from extra-parenchymal signals or to correct the evoked activation profile across cortical depths [30-36].

fMRI acquired with different contrasts and sub-millimeter resolution has enabled the function of the cerebral cortex to be sampled with column- and layer-specificity in the context of sensory, motor, visual and auditory tasks [15, 17-25, 37-39], and has shown the superficial layers of the neocortex to be predominantly involved in the processing of neuronal signals. This predominance is possibly due to fact that layer III is the main source and target of cortico-cortical connectivity [40], coupled with the higher synaptic density found there compared to the remaining cortical layers, and which is associated with higher receptor densities [1]. Importantly, a study focusing on the visual cortex reported correlations between the function of specific layers imaged with fMRI and particular EEG rhythms [41], reinforcing the potential for using fMRI to detect layer variability.

In contrast to task-related circuits, which are usually limited to specialized responses in a small portion of the cerebral cortex, during rest, cross-talk between distant cortical areas maintains a baseline neurological state [42]. Although the potential for using fMRI to sample cortical layers is clear, the limited brain coverage enforced by most existing high-resolution-fMRI schemes precludes the investigation of large-scale inter-regional depth-dependent connections. To date, only a few groups have reported fMRI acquisitions from the whole brain at ≤ 1 mm resolution [43-45] and, to our knowledge, only one study has intended to use laminar fMRI to uncover the cross-layer functional interactions that exist in the human brain during rest with a nominal spatial resolution of $0.8 \times 0.8 \times 0.8$ mm^3 [45].

Here, we applied TR-external EPIK, to identify the laminar signals from most of the cerebral cortex with a 0.63 mm iso-voxel size in healthy volunteers. It has been previously shown that EPIK [46-51] can offer higher spatial resolution in dynamic MR studies with comparable hemodynamic-response detection compared to routine EPI [52-56]. Moreover, the combination of TR-external phase correction with EPIK has been shown to offer a further enhancement of the spatial resolution[50, 57]. In this work, TR-external EPIK was optimized to almost entirely cover the human brain with 123 slices sampling voxel volumes of ~ 0.25 mm^3, estimated to enclose ~ 17500 neurons; for reference purposes, a 1 mm^3 voxel would enclose ~ 70000 neurons. The combination of smaller voxel size and near whole-brain coverage is a key feature of this work when compared to previous laminar fMRI studies. By adding pre-processing steps to correct for the potential bias of the GE sequence, e.g., using the phase component of the MR signal as a regressor, the acquired images allowed us to perform cortical depth dependent analysis of broad resting-state networking in the human brain.

2. MATERIALS AND METHODS

2.1. Subjects:

The functional data from thirteen healthy volunteers (eleven males and two females; age, 23-47 years; 12/13 right-handed, 1/13 left-handed [58]) were included in this study. Although eighteen subjects were originally measured, four of them were removed from the study due to the lack of/non-proper physiological recordings, and an additional set of data was removed after detecting high levels of motion. Hence, the structural scans of eighteen subjects were used for the anatomical study of the cortex but only data from thirteen subjects were included in the functional analysis. The experimental methods were approved by the local institutional review board (EK 346/17, RWTH Aachen University, Germany). MR-safety screening was performed on all subjects prior to MRI acquisition and informed written consent was obtained from all volunteers. Subjects were scanned in one single session for a period of ~55 min, which included two resting-state fMRI scans (rs-fMRI), one finger motor task fMRI scan (task-fMRI) and an MP2RAGE scan. A pneumatic belt was positioned around the subject's chest, and a pulse oximeter was placed on the 2nd, 3rd, or 4th finger of the left hand to control for potential interference of the physiological signals on the fMRI responses [59].

2.2. Experimental design:

In the rs-fMRI, subjects were asked to remain still, awake, with eyes closed and without thinking about anything in particular. In total, 172 volumes were acquired during the rs-fMRI (~10 min). For task-fMRI, subjects were asked to follow instructions on a projected screen and to perform flexion of the right index finger, without necessarily touching the thumb. The task was performed continuously at a comfortable pace (1-2 Hz, for most subjects) for 21 s and was repeated 12 times, alternated with 21 s of rest. In total, 148 volumes were obtained (4 s rest, [21 s task, 21 s rest] × 12) (~ 8,6 min). One subject was invited to participate in an additional scan session and first performed a finger motor task (4 s rest, [21 s task, 21 s rest] × 8), followed by a finger motor and sensory task, i.e., instructions were given to approach the right index finger towards the thumb involving touching (4 s rest, [21 s task, 21 s rest] × 8).

2.3. MRI data acquisition:

MRI data were collected on a Siemens Magnetom Terra 7T scanner with a 1-channel Tx / 32-channel Rx Nova Medical head coil. An anatomical MRI volume was acquired using an MP2RAGE sequence, TR/TE = 4300/2 ms, matrix = 256 × 376 × 400 (0.60 × 0.60 × 0.60 mm^3). Functional MRI data were obtained using gradient-echo EPI with keyhole (EPIK) combined with a TR-external EPI phase correction scheme (the sequence performance has been previously described elsewhere [50]), using two different acquisition protocols. In both protocols, TR/TE = 3500/22 ms, FA = 85°, partial Fourier = 5/8, 3-fold in-plane/3-fold inter-plane (multi-band) acceleration. B0 shimming was performed with a standard routine provided by the manufacturer. For protocol-1, matrix = 336 × 336 × 123 slices (0.63 × 0.63 × 0.63 mm^3). For protocol-2, matrix = 408 × 408 × 105 slices (0.51 × 0.51 × 1.00 mm^3). The main figures show results acquired with protocol-1 (i.e., isotropic voxels).

2.4. Data analysis:

A summarized pipeline of our pre-processing methods can be found in **Figure 1**. Briefly, cortical surfaces were extracted from the anatomical scan and used as a template to map the functional signals using Freesurfer (Martinos Center for Biomedical Imaging, Charlestown, MA). The average time course of 21 ROIs were extracted from each surface. Post-processing analysis included ICA-analysis, temporal correlation (i.e. functional connectivity), spectral decomposition, amplitude of low frequency fluctuations (ALFF), regional homogeneity (ReHo) and general linear model (GLM) analysis. The assessment of the cortical model (results in **Fig. 2**) is based on an excellent work by Kay et al. [29]. Pre-processing was done mainly on AFNI (Analysis of Functional NeuroImages, NIH, Bethesda, MD), and post-processing software included FSL (FMRIB Software Library, Oxford, UK), AFNI and Matlab (Mathworks, Natick, MA). Note that the term "surfaces" or "layers" employed through the manuscript should not be interpreted as histologically-defined cortical layers; instead, the terms are employed to refer to each of the six different cortical depths that are artificially generated by splitting the cortical thickness into five different compartments. A more detailed explanation of the methods used to generate the presented results can be found in the *Supplementary Material*.

3. RESULTS

3.1. Characterization of the cortical template for whole-brain laminar mapping

In a recent report, we have demonstrated the feasibility of using TR-external EPIK to assess fMRI activity over a large FOV with submillimeter spatial resolution [50]. The additional acquisition of a structural MP2RAGE sequence enabled us to produce a surface model of the cerebral cortex for each subject. Based on this model, it was possible to study brain activity at six different cortical depths, referred to hereafter as "layers" (different from the cytoarchitectonically-defined cortical layers) and specified as "white, +20%, +40%, +60%, +80% and pial", from the deepest to most superficial, respectively. These layers were used as a template for analysis of the functional data (see *Methods* and **Fig. 1**).

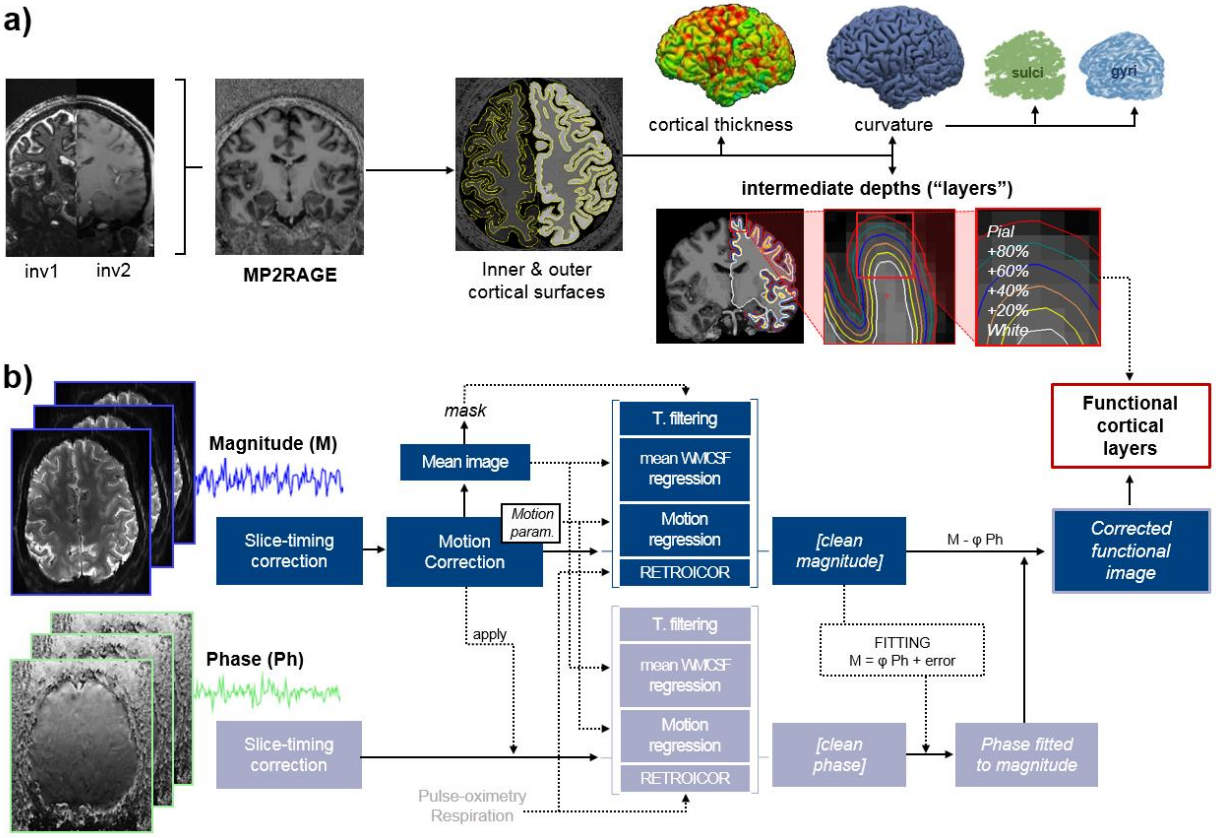

Figure 1. Main steps for pre-processing of the anatomical (a) and functional scans (b). a) *"inv1" and "inv2" indicate the first and second inversion contrast images of MP2RAGE. The T1-weighted MP2RAGE is used to segment the brain into gray matter, white matter, and cerebrospinal fluid (CSF). The cerebral cortex (outer brain gray matter) is further processed to extract its boundaries (outer or "pial" and inner or "white"). Several calculations can be performed based on these surfaces (e.g., thickness, curvature). Four additional surfaces are generated at equal spacing.* ***b)*** *Both the magnitude and phase images obtained with TR-external EPIK are subjected to a routine pre-processing pipeline including slice timing correction, motion correction, regression of physiological signals and temporal filtering. The pre-processed phase image is used to correct the magnitude image from vein-related bias. The corrected pre-processed magnitude functional image is then projected onto the six generated surfaces, in subject space, for laminar fMRI analysis.*

Figure 2 provides a characterization of the cortical model. In **Figure 2a**, an example of the distribution of sulci and gyri, i.e., the curvature of the cerebral cortex, and cortical thickness is provided on a representative coronal slice. The spatial resolution of each surface was assessed in sulci and gyri independently. As the cortical surfaces were generated by inflating the inner cortical boundary towards the pial space, a one-to-one correspondence between vertices existed across all surfaces; hence, the in-surface resolution varied depending on the depth and the curvature (for a visual example, see insets in **Fig. 2b**). The histograms in **Figure 2b** show the distribution of vertex-to-vertex distances at different cortical depths for gyri (blue) and sulci (green), in both cerebral hemispheres, as a mean ± standard deviation (SD), obtained from an 18-subject group. In agreement with previous work [29], it could be observed that, in gyri, the vertex-to-vertex distance increased from 'white' to 'pial'; on average, a sparse distance of 0.72±0.04 mm existed between the vertices in the pial surface, whereas this distance was 0.49±0.01 mm in the white surface, i.e., the surface spatial resolution improved with depth in gyri locations. In contrast, in sulci, the vertex-to-vertex distance decreased from 'white' to 'pial', with an average of 0.36±0.01 mm between consecutive vertices in the pial surface vs. 0.49±0.02 mm between the vertices of the deepest layer, i.e., outer surfaces were more densely sampled in sulci. This feature was observed in both the left and right hemispheres. The upper inset in **Figure 2b** exemplifies the larger vertex-to-vertex distance in the superficial layers of the cortical gyri, and the inset below exemplifies the larger distance between consecutive vertices in gyri compared to sulci. Cortical thickness was calculated in both cerebral hemispheres for 21 ROIs and for gyri and sulci in the whole cortex (**Fig. 2c**). Note that the analysis specific to gyri or sulci only considered the bottom 20% and top 20% curvature values, respectively (see *Methods*). Given that the cortical ribbon is thicker in the crown of gyri than in their walls or in the fundus of sulci [29] (**Fig. 2c**, blue bar vs. green bar), the layer-to-layer separation is greater at this position of the gyri (**Fig. 2d**, 0.62±0.02 mm between layers of cortical gyri vs. 0.40±0.01 mm in sulcal locations), which indicates that a higher signal contamination from neighboring layers can be expected in sulci, particularly in their fundus. Note that the in-depth resolution in the crown of gyri, i.e., the inter-layer distance, approximately corresponds to the voxel size employed in our fMRI protocol. Overall, across 18 subjects these robust cortical features were observed to be in agreement with the literature [29]. This suggests that the chosen subject-specific cortical model could be used as a reliable template to map functional signals and to study layer-based functional oscillations.

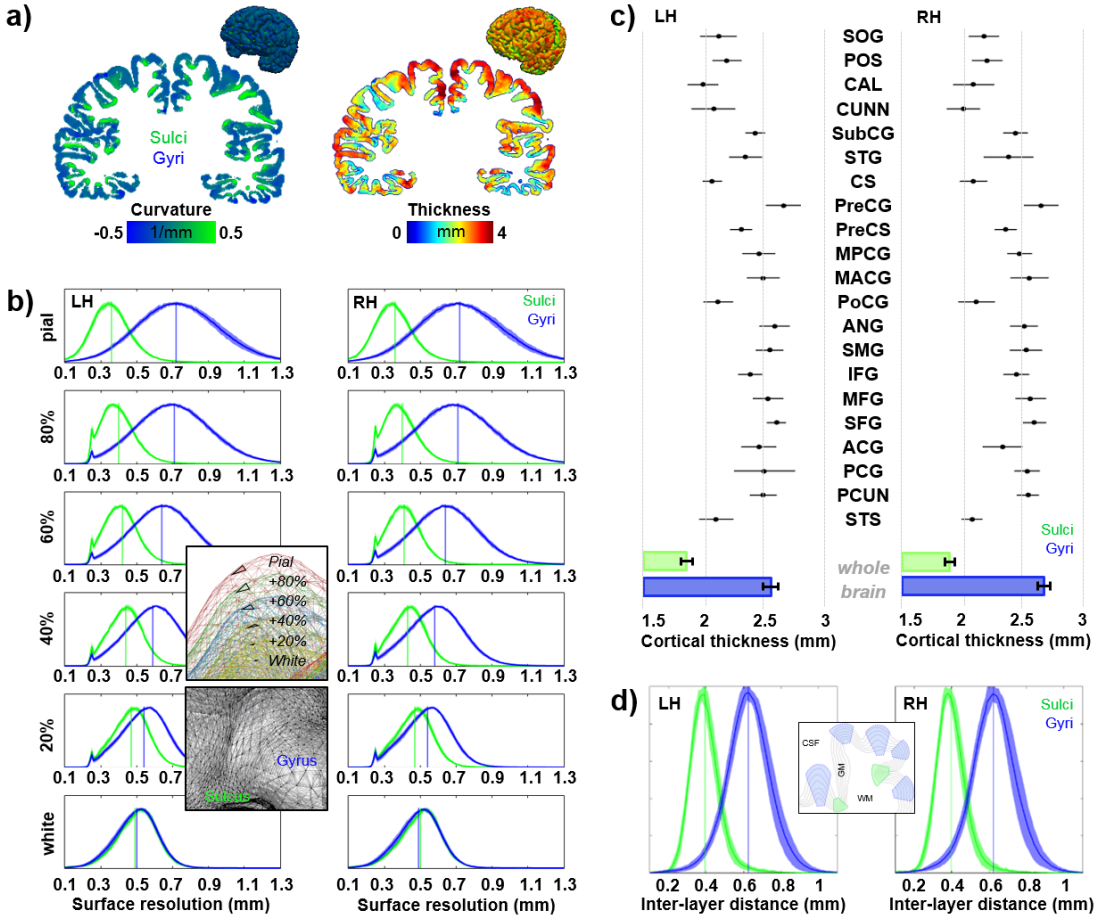

Figure 2. Evaluation of the cortical model. a) *Coronal slices showing the curvature and thickness of the cerebral cortex in a representative subject.* ***b)*** *Histograms showing the distribution of distances between two consecutive vertices at six different cortical depths, for locations corresponding to gyri (blue traces) or sulci (green traces), in both cerebral hemispheres. The insets show an example of the cortical surfaces in a gyrus (upper inset –an individual triangle is highlighted on each surface-) and of the pial surface over a sulcus and a gyrus (lower inset).* ***c)*** *Cortical thickness calculated in 21 ROIs and mean cortical thickness calculated from the whole brain in gyri and sulci, for both cerebral hemispheres (mean ±SD, N=18).* ***d)*** *Histograms showing the distribution of the distance between vertices located in contiguous layers (e.g., white–layer02, layer02-layer04; etc.), for gyri and sulci, in both cerebral hemispheres. Histogram plots show normalized mean ± SD (N=18).*

3.2. Depth-dependent evoked responses in the primary motor cortex (M1)

In order to prove the capabilities of TR-external EPIK for use in a laminar analysis of the whole brain, we first aimed to reproduce the results obtained in previous fMRI studies of finger-motor tasks. These results are characterized by a strong response in the upper layers of M1 and a second activation peak in the middle-deep layers when avoiding non-corrected GE-BOLD sequences [18-20]. A task-based fMRI protocol consisting of 12 epochs, alternating 21 s blocks of finger motion with 21 s blocks of rest, was conducted on each volunteer using a submillimeter-resolution protocol configured with TR-external EPIK; voxel size: 0.63 mm isotropic, matrix: 336 × 336, 123 slices (see protocol-1 in *Methods*). In agreement with the previous literature [18-20],

we observed a marked predominance of the BOLD response in the superficial layers of M1 (**Fig. 3**). A monotonous signal decrease from superficial to deep layers, typical in laminar GE-BOLD, was observed after averaging the beta coefficient within a portion of M1 (**Fig. 3a-c**, N=13), possibly partially reflecting a bias towards large venous vessels located on the surface (**Fig. S1**). However, when sampling the beta-map using only a few lines within area M1-4A [60], we were able to identify a bimodal response in multiple subjects and through several consecutive slices (**Fig. 3d, j-m**), which is typical of finger motor tasks finely assessed with line profiling in high-resolution schemes [18-20]. The specificity of laminar responses was further evaluated in one volunteer by comparing the activation profiles of two different tasks: movement-only, or movement + touch, i.e., somatomotion, or movement + somatosensation (**Fig. 3m**). While both tasks resulted in an initial activation peak in the superficial layers, the relatively salient response observed in deeper layers during movement was minimized and shifted towards more superficial layers upon addition of touch. Following a series of post-hoc correction steps to ameliorate the GE-BOLD signal bias towards pial vessels (see *Methods* and **Fig. S2**) [30, 31], the results obtained from the task-fMRI scans suggested that the submillimeter-resolution protocol obtained with TR-external EPIK is a reliable method for investigating whole-brain function with cortical depth specificity.

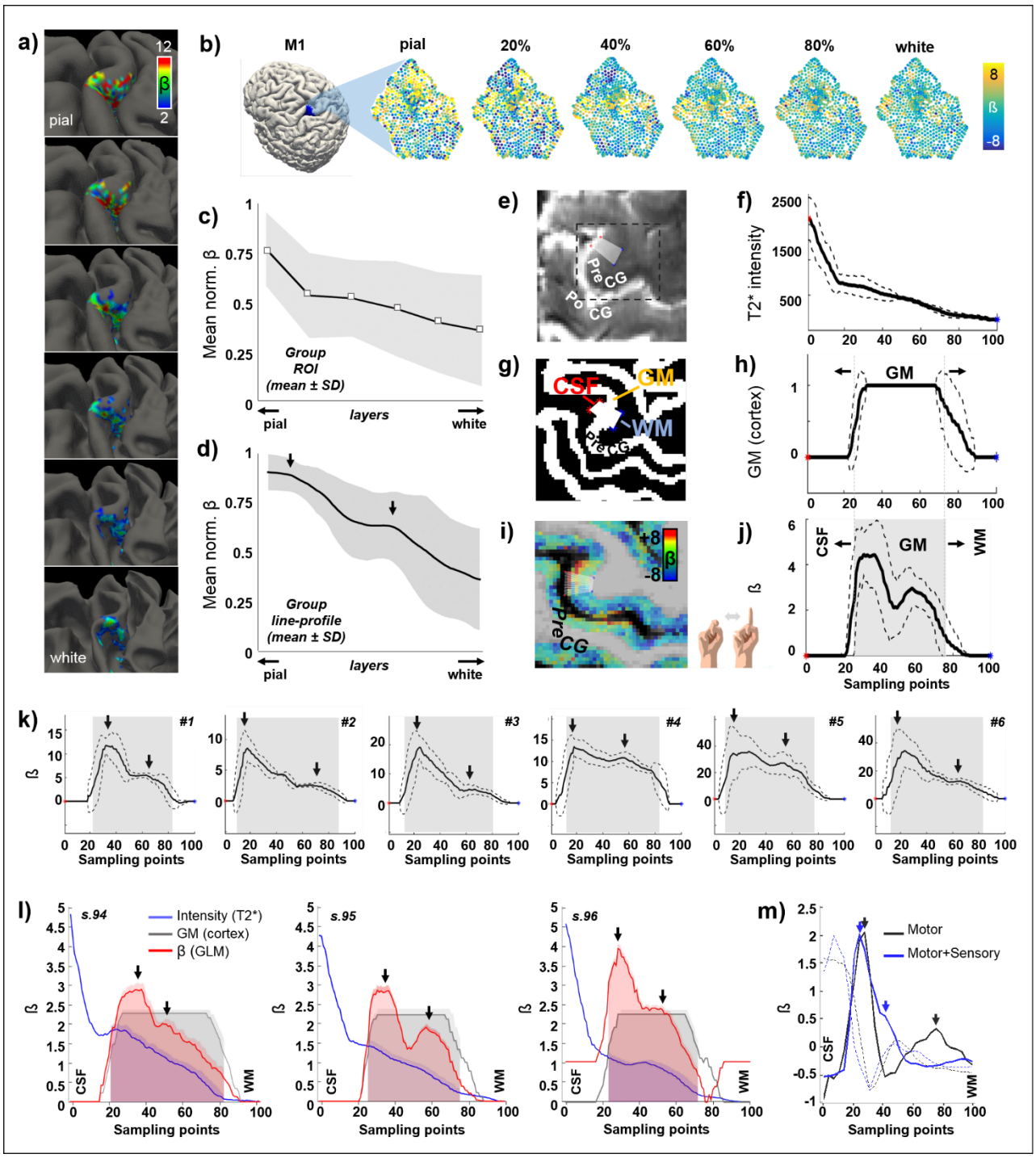

Figure 3. Cortical depth dependent motor task-evoked BOLD fMRI. a) *Six panels showing the surface beta-map of a selected ROI over different cortical depths of M1, resulting from a finger motor task in a representative subject.* ***b)*** *Flattened patches of the ROI in M1 extracted from six surfaces at different cortical depths.* ***c)*** *The plot shows the mean ±SD of the normalized beta-coefficient along six different cortical depths, from the pial surface of the brain towards the inner white matter boundary (N=13).* ***d)*** *Mean ±SD of the activation line-profiles, computed from the beta map of 13 subjects, using a line-profile method on a particular segment of M1 (computation explained through panels e)-j)).* ***e)*** *The figure shows part of a mean EPIK axial slice containing the pre-central gyrus (PreCG). The twenty overlaid sampling lines (in white) extend from the cerebrospinal fluid (CSF), covering the cortical thickness, up to the white matter (WM).* ***f)*** *Average line profile*

of the mean EPIK on the selected sampling region (the 20 lines on e)). Note the high intensity at the initial points (CSF, with long T2 constant). The discontinued lines above and below the solid line represent the mean ±SD. ***g)*** *Same region as in e), cropped from the segmented MP2RAGE, which identifies the cortical ribbon (in white color, labeled as gray matter (GM)).* ***h)*** *Line profile calculated from the sampling lines over the image in g).* ***i)*** *Beta coefficient map overlaid on the MP2RAGE.* ***j)*** *Profile of the beta coefficient along the selected lines crossing the finger area in the PreCG. Note the higher signal on superficial and middle layers of the cerebral cortex (double peak, typical of motor tasks). The gray-shaded area in j) represents the extent of the gray matter, with superficial layers (i.e., pial surface) on the left, near the CSF, and deep layers (i.e., white surface), on the right, near the white matter.* ***k)*** *Six subject-specific examples of line-profiles corresponding to a right finger motor task. The black arrows highlight the most salient signals across the cortical ribbon.* ***l)*** *Three examples showing the line profiles of the beta map in three consecutive slices (s94.s96) for one particular subject.* ***m)*** *Line profiles in a different volunteer performing either a finger movement only (black trace) or a finger movement involving touch (blue trace). Dashed lines indicate the intensity of the mean functional image for each task-fMRI scan, for spatial reference. PoCG post-central gyrus.*

3.3. Near whole-brain assessment of cortical depth dependent activity in resting-state fMRI

To investigate cross-layer interactions between distant cortical areas during rest, we acquired two additional task-negative fMRI scans from each subject, one using protocol-1, with 0.63 mm isotropic voxels, i.e., same as for the task-fMRI, and another using protocol-2, with higher in-plane resolution (0.51 × 0.51 mm^2) and thicker slices (1.00 mm) to maintain a reasonable SNR level. In order to reduce the dimensionality of our data (6 surfaces × ~ 290 000 vertices per hemisphere), we first segmented the cerebral cortex into 21 ROIs related to well-known brain networks: default mode, visual, sensory-motor, auditory, executive control and salience (**Fig. 4d** and **Table 1**). Having averaged the vertices within each ROI and each cortical layer in both cerebral hemispheres, we obtained 252 time courses from each fMRI scan (21 ROIs × six surfaces × two hemispheres). These were then subjected to several analysis methods. Following a frequency-power decomposition of the functional time courses, it was found that most cortical areas exhibit a higher level of activity in their superficial layers (**Fig. 4a**). This activity was observed to oscillate mostly within the range 0.01-0.03 Hz, which is in agreement with other non-laminar rs-fMRI studies focusing on cortical gray matter [61-64]. Integration of the signals fluctuating between 0.01 and 0.1 Hz, i.e., the typical range considered in rs-fMRI studies [65], provided a simplified measure of brain activity during rest, commonly denoted as the amplitude of low-frequency fluctuations (ALFF), which was assessed for each ROI and the six different cortical depths. The two panels in **Figure 4b** show the dependence of resting-state activity on cortical depth for each cerebral hemisphere, sorted by networks (in different colors, according to **Fig. 4d**) and differentiated into whole-ROIs, sulci or gyri of each ROI. The level of activity was observed to increase towards the surface of the cortex in most ROIs, irrespective of whether these were assessed in cortical gyri or cortical sulci (**Fig. 4e**), i.e., when approached by a linear fitting, the ALFF profile exhibited a positive slope (**Fig. 4f**). Gyri and sulci showed significantly different slopes ($p<0.005$) in the anterior midcingulate cortex (hub in the salience network), with gyri showing a steeper ALFF profile (green marker in **Fig. 4e**, middle vs. right panels); however, most of this ROI lies within the

crown of a gyrus, and hence the results may be biased by a low number of vertices considered in sulcal locations. The auditory network seemed to have steeper ALFF profiles in sulci, however the difference with respect to gyri was not significant (see purple marker in the same figure panels). The assessment of layer-specific regional homogeneity (ReHo) demonstrated network specific differences regarding the slope of this measure across the cortical thickness (see the different trends of lines in **Fig. 4c**). A significantly higher slope was observed in the ROIs of the visual network, compared to the other networks, in both hemispheres (see orange marker vs. other colors in **Fig. 4g**, $p<0.05$, when tested again every other network). Interestingly, while the ReHo slope was nearly flat or negative for most gyral locations, most ROIs exhibited a higher ReHo in the superficial layers of cortical sulci (**Fig. 4c**, sulci, represented by ● vs. gyri, represented by ▲), possibly due the proximity of neighbor points in the three-dimensional space of sulci compared to gyri. The differences in average ReHo slope between sulci and gyri (**Fig. 4h**) were significant in both hemispheres for most networks (e.g., in the left hemisphere, all ROIs with the exception of the anterior midcingulate cortex, demonstrated a p-value<0.05, with those in the default mode or the visual network showing $p<0.005$). The slope or gradient of ALFF and ReHo measures along the cortical thickness was significantly reduced when subjects were engaged in a motor task (**Fig. 4i**, **S3s** and **S3t**), i.e., the difference between superficial and deep layers, in terms of their signal amplitude and regional homogeneity, was significantly higher when subjects were in a resting-state. The assessment of functional amplitude and homogeneity with cortical depth specificity in our data suggested that the superficial layers of the cortex play a major factor in the maintenance of resting-state activity, which is significantly dampened during task performance.

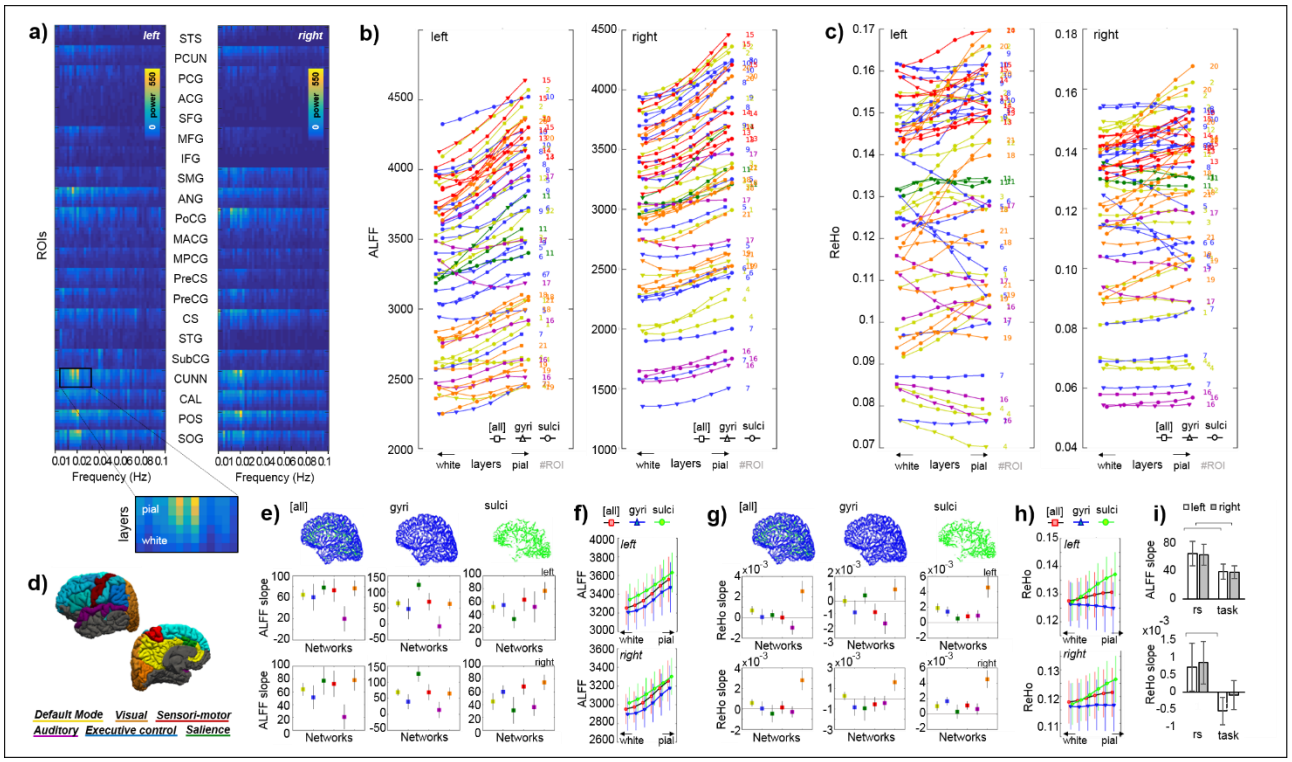

Figure 4. Cortical depth-dependent resting-state activity. ***a)*** *Mean layer-specific frequency-power decomposition of the BOLD signal in 21 ROIs (both cerebral hemispheres), averaged across 13 subjects.* ***b)*** *The plot shows the cortical depth dependence of the resting-state activity, measured as average ALFF, through*

all ROIs and both cerebral hemispheres. Numbers on the right of each line help tracing back each ROI (1 and 21 correspond to the first and the last ROI presented in a) –STS and SOG, respectively-). The line color indicates the network to which the ROIs are associated, and the squared, triangular or rounded symbols indicate whether the ROI was considered in its entirety, whether only the vertices corresponding to the most salient gyri in each ROI were considered, or whether only the vertices corresponding to the most salient sulcal locations in each ROI were considered, respectively. ***c)*** *Same plot as in b) but generated for the ReHo measures.* ***d)*** *The figure displays the regions that were included in the functional analysis, organized by network, over the surface of the brain (see* ***Table 1*** *for a detailed description of the ROIs included).* ***e)*** *Slope of the fitting line that approaches best the depth-varying ALFF for each cortical network.* ***f)*** *Average ALFF per layer, among all ROIs, for whole ROIs, sulci or gyri.* ***g, h)*** *Same plots as in e) and f) generated for the ReHo measures.* ***i)*** *The bar plot represents the average ALFF (above) and ReHo (below) slope computed for the resting-state and the task scan of 13 volunteers. Horizontal lines between two bars indicate significant differences ($p<0.05$). Error bars represent standard error of the mean.*

In addition to using ALFF to assess the "amount" of brain activity during rest, we investigated the connections between different brain regions at different depths of the cerebral cortex. To do so, a functional connectivity matrix was generated from each fMRI scan, which included the temporal correlation between all pairs of time courses, i.e., between the average time course of each region at each layer and that of every other region and layer (i.e., 252^2 cells). **Figure 5a** shows the connectivity matrix from a representative subject. The correlation values of the six layers in each ROI and the six layers of every other ROI were computed. For group analysis, the connectivity matrices of 13 subjects were averaged and subjected to a t-test for statistical thresholding. The resulting adjacency matrix was then used to generate a layer-specific, whole-brain connectivity graph. This was done for each scan acquired (**Fig. S3f, S3l & S3r)**. To facilitate the visual inspection of the depth-dependent connectivity graphs, the six assessed layers were grouped into "deep", "intermediate" and "superficial" layers, and connections were color-coded based on the pair of cortical depths involved, e.g., deep–deep connections were represented by yellow lines, intermediate–intermediate connections by red lines, deep-intermediate connections by orange lines, etc. In order to simplify the connectivity results, inter-regional connections were grouped per network. **Figure 5e-g** shows three versions of four connectivity graphs, with variable layer visibility, demonstrating the depth-specific significant connections within the default mode network, the executive control network, the sensory-motor network and the visual network, obtained from a resting-state scan acquired with protocol-1 (N=13). The same graphs were also computed from the task-based fMRI obtained with protocol-1 and the rs-fMRI obtained with protocol-2, which can be found in **Figure S4**. From a global-ROI perspective, i.e., independent of cortical depth, our data presented multiple significant connections that were in agreement with the volume-based resting-state network results derived from an ICA analysis; the volume-based examples and the corresponding depth-dependent profiles per ROI are shown in **Fig. 5h** and **Fig. S5**, respectively. The assessment of the cortical depth-dependent connectivity for each functional network, i.e., the overall temporal correlation between ROIs of the network at each cortical depth, demonstrates that intermediate and superficial layers govern most resting-state correlations (bell-shaped curve

with peak in intermediate or superficial layers, especially for the default-mode and visual networks, **Fig. 5c-d**). This resting-state connectivity preference was slightly shifted, during resting state, towards the infragranular layers in the executive control network, i.e. fronto-parietal connections (**Fig. 5c**, blue trace), which was evidenced, for instance, as stronger interhemispheric connections between intermediate layers compared to superficial layers of the middle frontal gyrus (orange lines in **Fig. 5f**: "Executive control").

During task performance, the network connections were, in general, slightly reduced (**Fig. S3l** vs. **S3f**) and some layer-specific relationships were altered (the task connectivity results are shown as supplementary material). For instance, during the motor task, the connectivity within the executive control network seemed to involve more superficial layers of the cortex (note the peak shift towards the right in the blue trace of **Fig. S3k**, compared to **Fig. S3e**); in contrast, more intermediate layers were involved in default mode network connectivity (yellow trace in **Fig. S3k**), contributing to a stronger correlation between the anterior cingulate cortices of both cerebral hemispheres, and a reduced interhemispheric connection of superior temporal areas (**Fig. S4a**, middle graph). The visual network showed increased intra-hemispheric connectivity during the visually cued motor task (**Fig. S4f**, middle graph) and the sensory-motor network showed decreased inter-regional connectivity, although central and post-central regions of the cortex as well as the supragranular layers of the left pre- and post-central gyrus were strongly connected, and the right pre-central area (gyrus and sulcus) showed synchronized activity in intermediate and infragranular depths (**Fig. S4d**, middle graph).

In most cases, connections involving deeper layers of the cortex were reduced in the resting-state networks assessed (**Fig. 5g**, compared to 5e or 5f). A connectivity analysis based on coherence instead of temporal correlation rendered similar results (**Fig. S6**). The similarity between the layer-specific connectivity graphs obtained from rs-fMRI using protocols 1 and 2 (**Fig. S3** and **S4)** suggests that the TR-external EPIK sequence is a reliable method for mapping cortical connections through the brain. Furthermore, the differences in connectivity obtained from the fMRI scans acquired with protocol-1 during rest or during task performance (**Fig. S3 and S4**) also demonstrate the sensitivity of TR-external EPIK for tracking brain state connectivity changes.

The average cross-layer connectivity is summarized in three matrices showing the average correlation between the layers of the ROIs in the left hemisphere (**Fig. 5b**, "Within LH"), the right hemisphere (**Fig. 5b**, "Within RH"), and the average inter-hemispheric correlation, i.e., layers of ROIs in the left hemisphere connecting with layers of ROIs in the right hemisphere (**Fig. 5b**, "Inter-hemispheric"). These matrices further suggested that the intermediate and superficial layers of the cerebral cortex are strongly involved in maintaining both intra- and interhemispheric connectivity. Note that the average connectivity between reciprocal layers (diagonal elements) was higher between hemispheres, possibly reflecting the connectivity between counterpart layers in opposite hemispheres. Similarly, when evaluating the ROI-specific connectivity per cortical depth (considering both, intra and inter-hemispheric connectivity).

The identification of stronger connections involving, mostly, the supragranular layers of the cortex is in agreement with previous reports demonstrating a higher level of activity and communication near the surface of the cortex in humans and non-human primates during rest [66, 67].

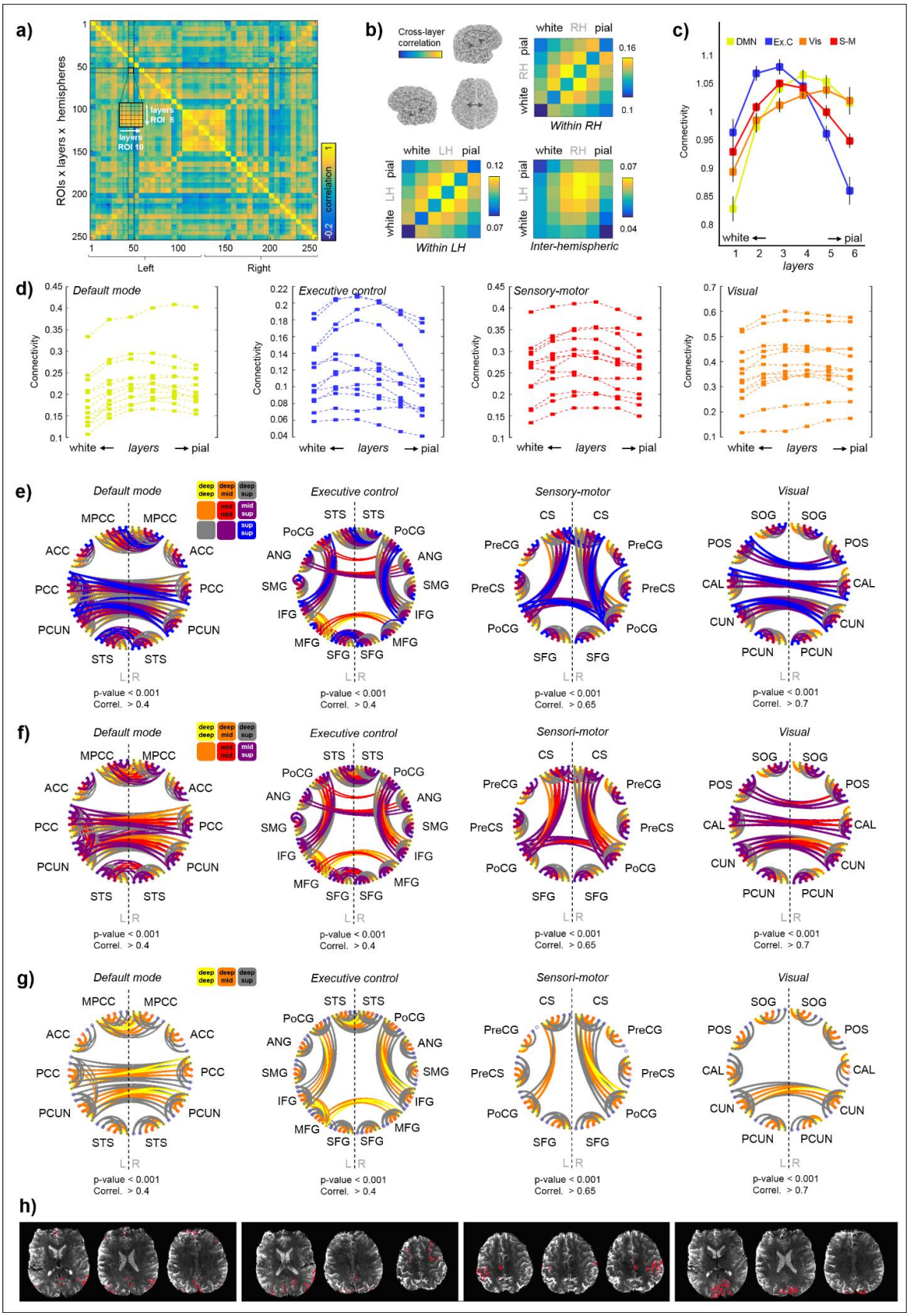

Figure 5. Cortical depth-dependent functional connectivity. a) *Representative connectivity matrix integrating the temporal correlation values between six cortical layers of 21 ROIs in both cerebral hemispheres.* ***b)*** *Average cross-layer connectivity within and between hemispheres.* ***c)*** *Cortical depth-specific global connectivity averaged in four resting-state networks. Error bars indicate ± standard error of the mean, N=13.* ***d)*** *Each of the four graphs shows the averaged connectivity for each functional network at each cortical depth for all subjects included in the analysis.* ***e)*** *Four graphs showing the layer-specific functional connections between ROIs engaged in four different brain networks. A legend is provided above the first graph. A version of these graphs hiding the top two superficial layers (i.e., only deep and intermediate layers are visible) and the two middle layers (i.e., only deep layers are visible) is provided in* ***f)*** *and* ***g)****, respectively.* ***h)*** *Below each set of connectivity graphs, three representative axial slices showing a volume-based ICA identification of the particular network are presented. In the case of the sensory-motor network, the three independent components reflecting left, bilateral and right sensory-motor network are shown.*

3.4 Cortical-depth assessment in the motor cortex during task performance and rest

An additional connectivity analysis in three regions that are engaged in motor processing exemplified some of the differences at the level of cortical layers that are associated to the brain state. Specifically, we extracted small patches from the left primary motor cortex (M1), left lateral premotor cortex (PreM) and left supplementary motor area (SMA), and evaluated the coherence between each pair of the layer-specific time courses, which reflects the similarity of both signals in terms of their frequency content. Coherence analysis generates a similarity measure that is less biased by particular events in time, compared to temporal correlations [64, 68, 69]; correlation analysis rendered similar results. The bottom graph in **Figure 6a** shows the layer-to-layer connectivity changes observed when subjects transited from a resting state to the performance of a motor task. We found that the connectivity between superficial and intermediate layers of M1 and superficial layers in SMA was significantly increased during finger movement ($p<0.001$, $N=13$). This demonstrates a layer-specific preference in communication during motor engagement.

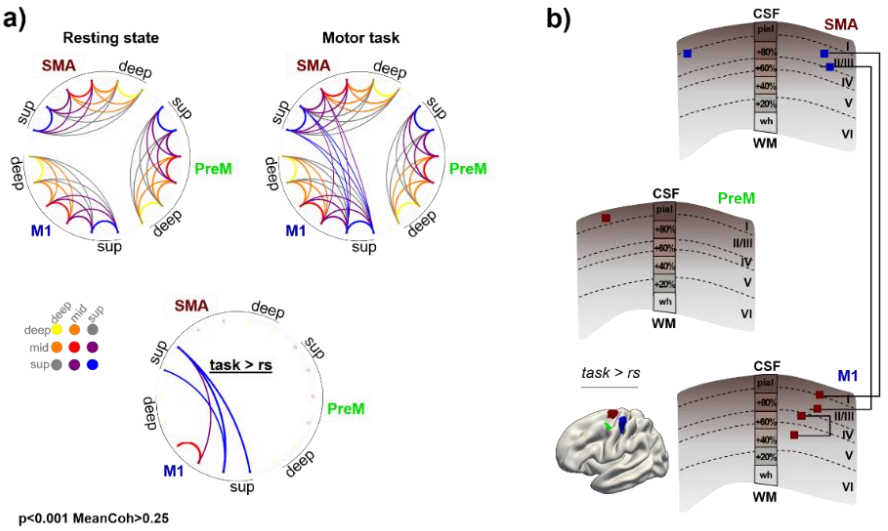

Figure 6. Coherence between cortical laminae of the motor system. a) *Coherence-based connectivity graphs in a left motor network during resting state and during performance of a motor task. The increased connectivity*

between layers during task performance was tested with a paired t-test and significant connections are shown in the graph below. ***b)*** *Summarized connectivity changes observed in the assessed motor network. In each of the three cortical sketches, the approximate location of the histological layers is indicated in dashed lines, with the artificially generated layers used in our study shown in the center as boxes (equally distributed along the cortical thickness).*

4. DISCUSSION

The layer-specific communication patterns across distant brain regions of the human brain have remained largely unexplored, mainly due to the reduced brain coverage afforded by most high-resolution methods. In this report, we employed a recently developed fMRI sequence (TR-external EPIK [50]) to address the question of how the different depths of the cerebral cortex participate in the maintenance of the resting-state in humans. We first obtained motor-evoked responses that reproduced the laminar results seen in the existing literature, and then provided a cortical-depth specific characterization of resting-state activity spanning multiple brain regions. We show that the amplitude of the resting state oscillations is larger in the superficial layers of the cortex, that the regional homogeneity is higher in the superficial layers of sulci but not gyri, and that the network connectivity is generally stronger between layers located in intermediate and superficial depths of the cortex, although particular weighting towards deeper cortical layers was observed in specific networks. Our results reveal the important role of the supragranular layers in resting-state connectivity in humans, which is in agreement with animal studies [10, 11].

In this study, we acquired two sets of rs-fMRI data for each subject within the same imaging session: one using isotropic voxels and the other using higher in-plane spatial resolution but with thicker slices. Both sets of data had voxels of similar volume (~ 0.25 mm^3). The resemblance between all functional measures assessed in both sets of the rs-fMRI data (**Fig. S3** and **S4**) suggests that both protocols were able to detect brain connectivity with layer-specificity to a similar level of performance. In both cases, the superficial layers exhibited the largest signal fluctuations and the intermediate and superficial layers were more strongly connected, with the exception of the executive control network, which showed strongest connections on the intermediate and deeper layers. Despite the agreement between both protocols, protocol-2 was better able to detect statistically significant connections (**Fig. S3r** compared to **S3f**, **Fig. S4**). This was possibly due to the increased SNR afforded by protocol-2 [50]. Moreover, protocol-2 conferred more complete brain coverage, which may be critical for particular applications where structures that are located at the base of the brain, e.g., hippocampus, brainstem, etc., are significant for the integrity of the study. Therefore, despite the non-isotropic voxel dimensions in protocol-2 (0.51 × 0.51 × 1.00 mm), it may be a better candidate than protocol-1 for whole-brain laminar fMRI. A more detailed technical description of both of the TR-external EPIK protocols can be found in reference [50].

In previous literature, a higher activation of superficial, i.e., supragranular, cortical layers has been observed in laminar rs-fMRI studies that have focused on a restricted FOV in the human brain [66], in non-human primates [67], and in rodents [11]. In contrast to the granular layer, which receives thalamo-cortical afferents, and the deeper, i.e., infragranular, layers, which mainly initiate efferent responses through subcortical and spinal projections, the superficial layers are the principal source and target of cortico-cortical regulatory communication [70-75]. Hereby, the deeper portion of layer III receives long distance feedforward projections, whereas its superficial portion, together with layer II, is targeted by long-distance feedback projections [40]. The present results support the supposition that superficial layers play a role in resting-state maintenance, as

resting-state networks mostly involve cortical areas [42, 76]. Although the literature upholds the results obtained from our resting-state analysis, i.e., predominant participation of the superficial layers, the GE nature of the sequence employed poses questions as to whether the recorded signal could be merely a reflection of a vascular-related superficial bias. While the amplitude of the signal was generally higher in the superficial layers (measured as ALFF), the connectivity results shown here demonstrate that the ability of the fMRI sequence to map layer-specific connections was not compromised, or at least it was not compromised to the extent of masking interactions occurring below the surface of the cortex. In fact, the connectivity measures peaked in intermediate or more superficial layers but rarely on the most external layer of the cortex. Besides, the fact that the layer-dependent signal amplitude, homogeneity and whole-brain connectivity were significantly altered upon task performance using exactly the same imaging protocol (**Fig. 2i**, **Fig. 6**, **Fig. S3**, **Fig. S4**) suggests that a vein-related bias, if present, was not the only factor accounting for the observed responses. Notwithstanding this assertion, the potential implications of using a GE-based sequence will be discussed in a later paragraph.

In comparison to the resting-state paradigm, the assessment of layer-specific correlations during task performance revealed a decreased number of functional connections (**Fig. S3l** vs. **S3f**), which is in agreement with the literature [77]. In contrast to the decreased functional connectivity of broad networks, the signal fluctuation in the left precentral gyrus, post-central gyrus and central sulcus (regions engaged in somatosensory and somatomotor processing) exhibited higher power during task performance compared to rest (**Fig. S3g** vs. **S3a**, see arrows), which is consistent with a more active primary motor cortex. The specificity of the evoked responses was demonstrated with distinct line profiles in the precentral gyrus, in response to somatomotion, with and without somatosensation (**Fig. 3m**). Finger movement resulted in activation of the superficial and, to a lesser extent, deeper layers, the latter possibly indicating signaling from premotor and supplementary motor cortices, also coinciding with cortical motor efferents towards pontomedullary or thalamic nuclei [11, 78]. Sensory processing triggered by the touch between two fingers produced activation in intermediate layers, possibly reflecting the modulation of the motor cortex by sensory cortical areas and afferents from the sensory thalamus [11, 78, 79]. The activation observed near the cortical surface may reflect, at least to a certain extent, a contribution from the venous network. However, superficial neuronal responses can be expected during performance of a motor task, as motor thalamic afferents modulate motor behavior in superficial and intermediate layers of the cortex, in a similar way as the sensory thalamic afferents upon addition of touch [78], which has also been observed in laminar studies [18]. The fact that evoked responses in the intermediate and deep layers (**Fig. 3j**) were detected in a line-profile analysis but not in the analysis of a bigger cortical patch, also responding to the motor task but exhibiting an upper → deeper trend only, demonstrates the specificity of the laminar responses on particular cortical regions and the overall preponderance of BOLD responses in the superficial layers in less specific evaluations.

Assuming a fair neuro-vascular coupling, the fMRI signal extracted from a cortical capillary network is a reliable indicator of neuronal activity. However, capillaries supplying blood to neurons flow in bigger ascending venules that run perpendicular to the cortex and disgorge into pial veins tangential to the surface of

the brain, and these veins influence the fMRI signal and can result in a bias towards the superficial layers of the cortex. The current study is based on GE-BOLD fMRI, which is known to be sensitive to changes in the macrovasculature; hence, it presents a less spatially-specific signal than other acquisition schemes, such as SE-BOLD fMRI, sensitive to oxygenation changes in the microvasculature only, vascular space occupancy fMRI (VASO), sensitive to vessel dilation, or cerebral blood flow-based fMRI (CBF), sensitive to flow changes. Due to the short T2 constant of blood at ultra-high field, BOLD-fMRI at 7T is only sensitive to the extra-vascular effect of the oxy/deoxy-hemoglobin ratio, in vessels of all sizes. Although the parenchymal vessels, i.e., venules of diameter < 25 μm, are detected by both SE- and GE-BOLD, these are often overshadowed in GE sequences by the influence of bigger veins running along the surface of the brain, which cause static perturbations in the magnetic field affecting the neighboring parenchymal tissue. Therefore, while SE-BOLD offers a fine localization of the activated parenchyma, GE-BOLD provides a mixed signal that is relevant to both small parenchymal vessels and macroscopic veins. To correct for this bias, we subtracted the time-varying phase component of the MR signal from each voxel's magnitude time course. The time-varying phase component is proportional to the frequency offset exhibited by the spins and hence, sensitive to the venous vasculature [30, 31]. As large vessels produce field inhomogeneities, spins processing in the neighboring parenchyma would produce changes in the phase component of the signal; in contrast, small randomly oriented vessels, e.g., in the capillary network within the gray matter, do not produce a net phase and hence, their derived signal remains intact. Although this method helps to improve the local specificity of BOLD, several biases could remain in the corrected data, such as those derived from motion correction or geometric distortions [80]; it is worth noting that the last ones are generally reduced in EPIK compared to conventional EPI [52]. Additionally, the frequency offsets derived from field inhomogeneities around vessels that are oriented parallel to the B0 field cannot be compensated for during the post-processing [81]. A few groups have demonstrated the dependence of laminar fMRI on the orientation of the cortex with respect to B0 [81, 82]. Although orientation bias can be critical for the dissection of the fMRI signal, this effect has been correlated with low frequency drift, motion and respiratory cycles, which were accounted for in our study, therefore diminishing the discussed effect. Moreover, most of our results were obtained from relatively big patches of cortex and through multiple ROIs, averaging vertices with different orientations within a cortical surface, and hence, although non-negligible, an orientation bias is not expected to have conditioned our results. However, a future model accounting for such an effect could determine the extent to which the curvature affects the laminar profiles at a whole-brain level.

In contrast to retrospective model-based approaches that reduce the superficial BOLD bias by applying temporal decomposition [36], linear detrending [32], normalization [33] or deconvolution [34, 35] to evoked fMRI data, the phase-based correction method employed here does not involve a priori assumptions about the behavior of the vascular dynamics across the cortical thickness and does not rely on the use of an evoked paradigm, offering a bias-free alternative to correct resting-state GE-fMRI data. Based on our results, this phase-based method [30] may constitute a rather conservative approach, i.e., the activity of the superficial layers was found to predominate almost ubiquitously (higher ALFF in upper layers of the cortex), however, connectivity analysis did identify laminar interactions in a cortical profile different from the linear gradient

that would be expected in purely macro-vascular measures, i.e., with a maximum on the surface, and the evoked responses were composed of two peaks, the latter located in deeper layers of the cortex, indicating a decent laminar sensitivity. Future studies employing GE-EPIK and SE-EPIK will investigate the possibility of complementing the phase-correction method with additional strategies to exploit the high SNR of GE-schemes with robust laminar specificity.

The vascular dependence of the fMRI signal remains one of the biggest challenges in laminar fMRI [83]. Signals obtained with BOLD contrast are not only conditioned by a physically-constrained laminar point-spread function, i.e., the fact that ascending venules spread the deep activation signals towards superficial layers [35, 84, 85],, but also by the varying physiological mechanisms underlying the BOLD response (CBF, CMRO2, CBV), which can modulate this point-spread function across cortical layers [84]. Despite the complexity of the model, laminar fMRI studies have even employed strategies that artificially sample the cortical depth with a number of points higher than the number of voxels across the cortical ribbon. This is appropriate under the assumption that the purpose of the study is tracking the trend of activation across the cortical depth and not to resolve the actual neuronal signal at any particular layer, which is indeed not possible, even with sufficient spatial resolution, given the facts discussed above. In this study, the number of depths used was equal to the number of histologically-defined layers in the neocortex; however, the layers in our model have been arbitrarily chosen to be equally spaced along the cortical thickness and have no direct relationship with the cortical cytoarchitecture, hence, our conclusions should be interpreted in terms of cortical depth only. Although some reports have chosen a smaller number of layers for their laminar assessment (e.g., 3 [44]), which simplifies the analysis and confers layers with a greater independence, others have shown that a greater number of depths (e.g., 20 [18]), enables clearer detection of cortical responses, despite the fact that this strategy involves a greater dependence on neighbor signals. In addition, the last scheme also poses an important challenge in whole-brain studies due to the high computational demands of the analysis procedure (see discussion below).

Irrespective of the number of layers, ambitious whole-brain laminar fMRI studies should assure perfect co-registration between the anatomical reference scan and the functional data. Previous reports have shown the possibility of integrating T1 contrast within a high-resolution fMRI sequence (e.g., [18], acquired during VASO), which allows a 1:1 relationship between the anatomical and functional scans, mitigating any co-registration concern. This option was not yet available in the current study. Nevertheless, in this work, we achieved acceptable co-registration in the majority of the brain by using manual rigid transformations (**Fig. S7**), which proved to be more reliable than the transformations rendered by non-linear automatic registration tools. In addition, the improved robustness against geometric distortions in EPIK [52] is expected to yield fewer co-registration errors, compared to the common EPI, between the functional scans and the anatomical scans (e.g., MR2RAGE). However, particular areas in different subjects remained poorly co-registered and needed to be masked out to ensure a proper laminar analysis. In the future, TR-external EPIK will be modified

to provide a T1 contrast, which will avoid data loss, reduce the pre-processing time and, more importantly, will alleviate the potential concerns relating to co-registration.

In this work, we employed TR-external EPIK to map the majority of the brain with a voxel resolution of 0.63 × 0.63 × 0.63 mm^3 or 0.51 × 0.51 × 1.00 mm^3. In addition to the challenge in terms of sequence design, the resulting matrix size imaged by TR-external EPIK (336 × 336 × 123 or 408 × 408 × 108) presents important computational limitations, such as the relatively large memory required (minimum storage space: ~ 6 Gb per 4D-volume; RAM: ≥ 32Gb for many pre-processing steps) and long processing times. After pre-processing, analysis of the cortical surfaces with numerical computing environments such as Matlab is, again, conditioned by the number of vertices to be processed, and therefore, the greater the number of layers, the higher the computational demands. For instance, one cortical surface covered by protocol-1 contained ~ 290,000 vertices, which means that the six surfaces obtained from both hemispheres involved the analysis of ~ 3,480,000 vertices, each of them consisting of a 168-point time course. In this work, in order to adjust the computational demands to those of a standard scientific workstation, the first step in most of the layer-specific functional analysis was to average all vertices specific to one layer within one ROI. Given that the laminar performance of the cortex can be highly localized, some events might be overlooked when using an ROI-based analysis to identify particular behaviors; hence, the use of supercomputing resources to assess vertex-specific measures becomes highly desirable to exploit the capabilities of the acquired data.

5. CONCLUSION

This study adopted a sequence offering exceptional resolution (~ 0.25 mm^3 voxels) to map laminar functional dynamics in a 7T scanner with near whole-brain mapping in healthy volunteers. We investigated the dependence of common rs-fMRI measures such as ALFF, ReHo and functional connectivity on cortical depth, which has emerged as a new dimension to be explored in the human brain. Our results indicate that the intermediate and superficial layers play a critical role in the maintenance of the resting-state and that the chosen sequence can help identifying functional differences related to brain state changes, here demonstrated as changes in the laminar connectivity during task compared to rest. This work sets the basis for novel investigations of the resting-state, in particular in neuro-psychological diseases with cortical depth specificity.

ACKNOWLEDGEMENTS

We thank Dr Michael Schwerter for guidance in the phase-signal processing; Ms Elke Bechholz and Ms Anita Köth for technical support; Ms Rick Claire, for manuscript corrections, and the fMRI volunteers for their excellent cooperation.

636 **Table 1. Regions of interest.**

Abb. ROI	Full ROI name	Related network(s)
MPCC	Posterior Midcingulate Cortex	DMN
ACC	Anterior Cingulate Cortex	DMN
PCC	Posterior Cingulate Cortex	DMN
PCUN	Precuneus	DMN & VISUAL
STS	Superior Temporal Sulcus	DMN & EXEC
PoCG	Post-Central Gyrus	EXEC & SM
ANG	Inferior Parietal - angular	EXEC
SMG	Inferior Parietal - supramarginal	EXEC
IFG	Inferior Frontal G&S	EXEC
MFG	Middle Frontal Gyrus	EXEC
SFG	Superior Frontal G&S	EXEC & SM
SOG	Superior Occipital Gyrus	VISUAL
POS	Parieto-occipital Sulcus	VISUAL
CAL	Calcarine	VISUAL
CUN	Cuneus	VISUAL
CS	Central Sulcus	SM
PreCG	Pre-Central Gyrus	SM
PreCS	Pre-Central Sulcus	SM
STG	Superior Temporal Gyrus	AUDITORY
SubCG	Subcentral G&S	AUDITORY
MACG	Anterior Midcingulate Cortex	SALIENCE

637 **Table 1.** DMN: default mode network; EXEC: executive control network; SM: sensory-motor
638 network.

References:

1. Palomero-Gallagher, N. and K. Zilles, *Cortical layers: Cyto-, myelo-, receptor- and synaptic architecture in human cortical areas.* Neuroimage, 2019. **197**: p. 716-741.
2. Thomson, A.M. and A.P. Bannister, *Interlaminar connections in the neocortex.* Cereb Cortex, 2003. **13**(1): p. 5-14.
3. Larkum, M.E., et al., *A Perspective on Cortical Layering and Layer-Spanning Neuronal Elements.* Front Neuroanat, 2018. **12**: p. 56.
4. Michelson, N.J. and T.D.Y. Kozai, *Isoflurane and ketamine differentially influence spontaneous and evoked laminar electrophysiology in mouse V1.* J Neurophysiol, 2018. **120**(5): p. 2232-2245.
5. Krupa, D.J., et al., *Layer-specific somatosensory cortical activation during active tactile discrimination.* Science, 2004. **304**(5679): p. 1989-92.
6. Adesnik, H. and A. Naka, *Cracking the Function of Layers in the Sensory Cortex.* Neuron, 2018. **100**(5): p. 1028-1043.
7. Ayaz, A., et al., *Layer-specific integration of locomotion and sensory information in mouse barrel cortex.* Nat Commun, 2019. **10**(1): p. 2585.
8. Scott, B.B., et al., *Imaging Cortical Dynamics in GCaMP Transgenic Rats with a Head-Mounted Widefield Macroscope.* Neuron, 2018. **100**(5): p. 1045-1058 e5.
9. Csercsa, R., et al., *Laminar analysis of slow wave activity in humans.* Brain, 2010. **133**(9): p. 2814-29.
10. Whitesell, J.D., et al., *Regional, Layer, and Cell-Type-Specific Connectivity of the Mouse Default Mode Network.* Neuron, 2021. **109**(3): p. 545-559 e8.
11. Weiler, N., et al., *Top-down laminar organization of the excitatory network in motor cortex.* Nat Neurosci, 2008. **11**(3): p. 360-6.
12. Logothetis, N.K., et al., *Neurophysiological investigation of the basis of the fMRI signal.* Nature, 2001. **412**(6843): p. 150-7.
13. Logothetis, N.K., *The neural basis of the blood-oxygen-level-dependent functional magnetic resonance imaging signal.* Philos Trans R Soc Lond B Biol Sci, 2002. **357**(1424): p. 1003-37.
14. Ogawa, S., et al., *Brain magnetic resonance imaging with contrast dependent on blood oxygenation.* Proc Natl Acad Sci U S A, 1990. **87**(24): p. 9868-72.
15. Yu, X., et al., *Deciphering laminar-specific neural inputs with line-scanning fMRI.* Nat Methods, 2014. **11**(1): p. 55-8.
16. Lawrence, S.J.D., et al., *Laminar fMRI: Applications for cognitive neuroscience.* Neuroimage, 2019. **197**: p. 785-791.
17. Guidi, M., et al., *Lamina-dependent calibrated BOLD response in human primary motor cortex.* Neuroimage, 2016. **141**: p. 250-261.
18. Huber, L., et al., *High-Resolution CBV-fMRI Allows Mapping of Laminar Activity and Connectivity of Cortical Input and Output in Human M1.* Neuron, 2017. **96**(6): p. 1253-1263 e7.
19. Chai, Y., et al., *Integrated VASO and perfusion contrast: A new tool for laminar functional MRI.* Neuroimage, 2020. **207**: p. 116358.
20. Huber, L., et al., *Cortical lamina-dependent blood volume changes in human brain at 7 T.* Neuroimage, 2015. **107**: p. 23-33.
21. Ress, D., et al., *Laminar profiles of functional activity in the human brain.* Neuroimage, 2007. **34**(1): p. 74-84.
22. Polimeni, J.R., et al., *Laminar analysis of 7T BOLD using an imposed spatial activation pattern in human V1.* Neuroimage, 2010. **52**(4): p. 1334-46.
23. Kashyap, S., et al., *Resolving laminar activation in human V1 using ultra-high spatial resolution fMRI at 7T.* Sci Rep, 2018. **8**(1): p. 17063.

24. van Mourik, T., et al., *Laminar signal extraction over extended cortical areas by means of a spatial GLM.* PLoS One, 2019. **14**(3): p. e0212493.
25. De Martino, F., et al., *Frequency preference and attention effects across cortical depths in the human primary auditory cortex.* Proc Natl Acad Sci U S A, 2015. **112**(52): p. 16036-41.
26. Lu, H., et al., *Functional magnetic resonance imaging based on changes in vascular space occupancy.* Magn Reson Med, 2003. **50**(2): p. 263-74.
27. Huber, L., et al., *Ultra-high resolution blood volume fMRI and BOLD fMRI in humans at 9.4T: Capabilities and challenges.* Neuroimage, 2018. **178**: p. 769-779.
28. Poplawsky, A.J., et al., *Layer-Specific fMRI Responses to Excitatory and Inhibitory Neuronal Activities in the Olfactory Bulb.* J Neurosci, 2015. **35**(46): p. 15263-75.
29. Kay, K., et al., *A critical assessment of data quality and venous effects in sub-millimeter fMRI.* Neuroimage, 2019. **189**: p. 847-869.
30. Menon, R.S., *Postacquisition suppression of large-vessel BOLD signals in high-resolution fMRI.* Magn Reson Med, 2002. **47**(1): p. 1-9.
31. Curtis, A.T., R.M. Hutchison, and R.S. Menon, *Phase based venous suppression in resting-state BOLD GE-fMRI.* Neuroimage, 2014. **100**: p. 51-9.
32. Fracasso, A., et al., *Laminar imaging of positive and negative BOLD in human visual cortex at 7T.* Neuroimage, 2018. **164**: p. 100-111.
33. Kashyap, S., et al., *Impact of acquisition and analysis strategies on cortical depth-dependent fMRI.* Neuroimage, 2018. **168**: p. 332-344.
34. Heinzle, J., et al., *A hemodynamic model for layered BOLD signals.* Neuroimage, 2016. **125**: p. 556-570.
35. Markuerkiaga, I., M. Barth, and D.G. Norris, *A cortical vascular model for examining the specificity of the laminar BOLD signal.* Neuroimage, 2016. **132**: p. 491-498.
36. Kay, K., et al., *A temporal decomposition method for identifying venous effects in task-based fMRI.* Nat Methods, 2020. **17**(10): p. 1033-1039.
37. Siero, J.C., et al., *Cortical depth-dependent temporal dynamics of the BOLD response in the human brain.* J Cereb Blood Flow Metab, 2011. **31**(10): p. 1999-2008.
38. Muckli, L., et al., *Contextual Feedback to Superficial Layers of V1.* Curr Biol, 2015. **25**(20): p. 2690-5.
39. Yacoub, E., N. Harel, and K. Ugurbil, *High-field fMRI unveils orientation columns in humans.* Proc Natl Acad Sci U S A, 2008. **105**(30): p. 10607-12.
40. Zilles, K. and M. Catani, *Cerebral hemispheres*, in *Gray's Anatomy*. 2020.
41. Scheeringa, R., et al., *The relationship between oscillatory EEG activity and the laminar-specific BOLD signal.* Proc Natl Acad Sci U S A, 2016. **113**(24): p. 6761-6.
42. Raichle, M.E., et al., *A default mode of brain function.* Proc Natl Acad Sci U S A, 2001. **98**(2): p. 676-82.
43. De Martino, F., et al., *Whole brain high-resolution functional imaging at ultra high magnetic fields: an application to the analysis of resting state networks.* Neuroimage, 2011. **57**(3): p. 1031-44.
44. Sharoh, D., et al., *Laminar specific fMRI reveals directed interactions in distributed networks during language processing.* Proc Natl Acad Sci U S A, 2019. **116**(42): p. 21185-21190.
45. Huber, L., et al., *Layer-dependent functional connectivity methods.* Prog Neurobiol, 2020: p. 101835.
46. Shah, N.J., Zilles, K., *Verfahren zur Untersuchung eines Objektes mittels Erfassung des Ortsfrequenzraumes*. 2003.
47. Shah NJ, a.Z.K., *Imaging process in the spatial frequency space and useful for examining the properties of object*. 2004.
48. Zaitsev, M., K. Zilles, and N.J. Shah, *Shared k-space echo planar imaging with keyhole.* Magn Reson Med, 2001. **45**(1): p. 109-17.
49. Zaitsev, M., et al., *Dual-contrast echo planar imaging with keyhole: application to dynamic contrast-enhanced perfusion studies.* Phys Med Biol, 2005. **50**(19): p. 4491-505.

50. Yun, S., P. Pais-Roldán, and N.J. Shah. *Detection of Cortical Depth-dependent Functional Activation using Whole-brain, Half-millimetre Resolution EPIK at 7T*. in *ISMRM*. 2020. Paris, France.
51. Yun, S.D. and N.J. Shah, *Analysis of EPI phase correction with low flip-angle excitation to reduce the required minimum TE: Application to whole-brain, submillimeter-resolution fMRI at 3 T.* Magn Reson Med, 2020. **84**(3): p. 1416-1429.
52. Yun, S.D., et al., *Parallel imaging acceleration of EPIK for reduced image distortions in fMRI.* Neuroimage, 2013. **73**: p. 135-43.
53. Yun, S.D. and N.J. Shah, *Whole-brain high in-plane resolution fMRI using accelerated EPIK for enhanced characterisation of functional areas at 3T.* PLoS One, 2017. **12**(9): p. e0184759.
54. Caldeira, L.L., et al., *Dynamic susceptibility contrast parametric imaging using accelerated dual-contrast echo planar imaging with keyhole.* J Magn Reson Imaging, 2019. **50**(2): p. 628-640.
55. Shah, N.J., N.A. da Silva, and S.D. Yun, *Perfusion weighted imaging using combined gradient/spin echo EPIK: Brain tumour applications in hybrid MR-PET.* Hum Brain Mapp, 2019.
56. Yun, S.D., et al., *Evaluating the Utility of EPIK in a Finger Tapping fMRI Experiment using BOLD Detection and Effective Connectivity.* Sci Rep, 2019. **9**(1): p. 10978.
57. Yun, S. and N.J. Shah, *Full-FOV, Whole-brain, Half-millimetre Resolution fMRI at 7T using Accelerated multi-band EPIK with TR-external Phase Correction*, in *27th Annual Meeting of ISMRM*. 2019: Montreal, Canada.
58. Schweisfurth, M.A., et al., *Comparison of fMRI Digit Representations of the Dominant and Non-dominant Hand in the Human Primary Somatosensory Cortex.* Front Hum Neurosci, 2018. **12**: p. 492.
59. Glover, G.H., T.Q. Li, and D. Ress, *Image-based method for retrospective correction of physiological motion effects in fMRI: RETROICOR.* Magn Reson Med, 2000. **44**(1): p. 162-7.
60. Geyer, S., et al., *Two different areas within the primary motor cortex of man.* Nature, 1996. **382**(6594): p. 805-7.
61. Zuo, X.N., et al., *The oscillating brain: complex and reliable.* Neuroimage, 2010. **49**(2): p. 1432-45.
62. Xue, S.W., et al., *Different neural manifestations of two slow frequency bands in resting functional magnetic resonance imaging: a systemic survey at regional, interregional, and network levels.* Brain Connect, 2014. **4**(4): p. 242-55.
63. Yuen, N.H., N. Osachoff, and J.J. Chen, *Intrinsic Frequencies of the Resting-State fMRI Signal: The Frequency Dependence of Functional Connectivity and the Effect of Mode Mixing.* Front Neurosci, 2019. **13**: p. 900.
64. Bajaj, S., et al., *Oscillatory motor network activity during rest and movement: an fNIRS study.* Front Syst Neurosci, 2014. **8**: p. 13.
65. Murphy, K., R.M. Birn, and P.A. Bandettini, *Resting-state fMRI confounds and cleanup.* Neuroimage, 2013. **80**: p. 349-59.
66. Guidi, M., et al., *Cortical laminar resting-state signal fluctuations scale with the hypercapnic blood oxygenation level-dependent response.* Hum Brain Mapp, 2020. **41**(8): p. 2014-2027.
67. Mishra, A., et al., *Functional connectivity with cortical depth assessed by resting state fMRI of subregions of S1 in squirrel monkeys.* Hum Brain Mapp, 2019. **40**(1): p. 329-339.
68. Sun, F.T., L.M. Miller, and M. D'Esposito, *Measuring interregional functional connectivity using coherence and partial coherence analyses of fMRI data.* Neuroimage, 2004. **21**(2): p. 647-58.
69. Li, K., et al., *Review of methods for functional brain connectivity detection using fMRI.* Comput Med Imaging Graph, 2009. **33**(2): p. 131-9.
70. Moerel, M., et al., *Processing complexity increases in superficial layers of human primary auditory cortex.* Sci Rep, 2019. **9**(1): p. 5502.

71. D'Souza, R.D. and A. Burkhalter, *A Laminar Organization for Selective Cortico-Cortical Communication.* Front Neuroanat, 2017. **11**: p. 71.
72. Rubio-Garrido, P., et al., *Thalamic input to distal apical dendrites in neocortical layer 1 is massive and highly convergent.* Cereb Cortex, 2009. **19**(10): p. 2380-95.
73. Larkum, M.E., *The yin and yang of cortical layer 1.* Nat Neurosci, 2013. **16**(2): p. 114-5.
74. Sempere-Ferrandez, A., S. Martinez, and E. Geijo-Barrientos, *Synaptic mechanisms underlying the intense firing of neocortical layer 5B pyramidal neurons in response to cortico-cortical inputs.* Brain Struct Funct, 2019. **224**(4): p. 1403-1416.
75. Rolls, E.T. and W.P.C. Mills, *Computations in the deep vs superficial layers of the cerebral cortex.* Neurobiol Learn Mem, 2017. **145**: p. 205-221.
76. Heine, L., et al., *Resting state networks and consciousness: alterations of multiple resting state network connectivity in physiological, pharmacological, and pathological consciousness States.* Front Psychol, 2012. **3**: p. 295.
77. Jurkiewicz, M.T., A.P. Crawley, and D.J. Mikulis, *Is Rest Really Rest? Resting-State Functional Connectivity During Rest and Motor Task Paradigms.* Brain Connect, 2018. **8**(5): p. 268-275.
78. Hooks, B.M., et al., *Organization of cortical and thalamic input to pyramidal neurons in mouse motor cortex.* J Neurosci, 2013. **33**(2): p. 748-60.
79. Mao, T., et al., *Long-range neuronal circuits underlying the interaction between sensory and motor cortex.* Neuron, 2011. **72**(1): p. 111-23.
80. Bause, J., et al., *Impact of prospective motion correction, distortion correction methods and large vein bias on the spatial accuracy of cortical laminar fMRI at 9.4 Tesla.* Neuroimage, 2019. **208**: p. 116434.
81. Viessmann, O., et al., *Dependence of resting-state fMRI fluctuation amplitudes on cerebral cortical orientation relative to the direction of B0 and anatomical axes.* Neuroimage, 2019. **196**: p. 337-350.
82. Baez-Yanez, M.G., et al., *The impact of vessel size, orientation and intravascular contribution on the neurovascular fingerprint of BOLD bSSFP fMRI.* Neuroimage, 2017. **163**: p. 13-23.
83. Uludag, K. and P. Blinder, *Linking brain vascular physiology to hemodynamic response in ultra-high field MRI.* Neuroimage, 2018. **168**: p. 279-295.
84. Havlicek, M. and K. Uludag, *A dynamical model of the laminar BOLD response.* Neuroimage, 2020. **204**: p. 116209.
85. Marquardt, I., et al., *Cortical depth profiles of luminance contrast responses in human V1 and V2 using 7 T fMRI.* Hum Brain Mapp, 2018. **39**(7): p. 2812-2827.